Computational study of effect of transient fluid force on composite structures submerged in water

Young W. Kwon* and Scott C. Knutton
Dept. of Mechanical & Aerospace Engineering, Naval Postgraduate School, Monterey, CA 93943, USA

ABSTRACT
This study investigated the effect of the initial transient hydrodynamic loading on dynamic responses of composite structures which move under water from the rest condition to a steady-state velocity for a given time duration with different acceleration profiles. Numerical analyses were conducted including the fluid-structure interaction. The computational model was validated against an experimental data, and various cases were examined numerically. The cases include various transient velocities of the structure, fluid boundary conditions, structural geometric configurations and material properties. The results showed that the peak fluid pressure and the resultant stresses in the composite structures are dependent on most of those parameters significantly. The maximum stresses under transient hydrodynamic loading could be an order of magnitude larger than those stresses under the final steady-state loading. A lighter composite structure experienced greater stresses and strains while the fluid pressure did not have any noticeable change under the same flow condition.

Keywords: Hydrodynamic loading, Fluid-structure interaction, Dynamic analysis of composite

1. INTRODUCTION

When a solid body moves inside water, a drag force occurs and it resists to the motion of the solid body. Additionally, the fluid force induces stress and strain in a deformable body. There has been extensive research to measure and compute the drag forces around solid bodies [1–4]. Most of the studies investigated steady state flows over rigid solids. Virtually every marine structure is subjected to velocity changes during its service period. For example, stationary offshore structures are subjected to changing currents while moving marine structures have changes in velocity during their operations. Thus, there is always transient fluid loading applied to a marine structure during its service period. Transient flows generally produce much greater fluid forces than steady state flows, which also results in larger stresses and strains in a deformable structure.

There are studies on transient fluid loading, for example as in Refs. [5–10]. However, most of the studies did not include the flexibility of the solid body. In other words, solid structures were considered as rigid. Some studied the fluid loading such as sloshing and water hammer on flexible structures [11–15]. When polymer composite structures are subjected to transient fluid loading, the effect of structural flexibility on the flow cannot be neglected. In other words, the effect of the fluid-structure interaction becomes significant for

*Corresponding Author: E-mail: ywkwon@Nps.edu

polymer composite structures because mass densities of the composite materials are very comparable to the water density. [16–19]

While there is a growing desire to increase use of composite materials in marine applications, these structures must still withstand the same hydrodynamic and impact forces withstood by steel and other commonly used materials. This poses a unique engineering challenge of designing a marine structure fabricated from a composite material to meet the rigorous demands.

This study examined the hydrodynamic pressure loading on polymer composite structures submerged in water with transient motion. In order to simplify the model of the study, transient flow around a composite structure was investigated instead of a moving structure in stationary water. The emphasis of the study was placed on investigation of the resultant stresses and strains in composite structures. A series of parametric studies were conducted for various acceleration cases, depth from free surface of water, structural geometric configurations and material properties using the finite element analysis of fluid-structure interaction.

The next section describes the computer models used in the study, which is followed by the verification of the model using an experimental study. Then, each case study for a series of parametric investigation is presented, and the results for each case study are discussed. Finally, summary and conclusions are provided.

2. DESCRIPTION OF COMPUTATIONAL MODELS

In this study, the fluid-structure interaction was modeled using a program called ANSYS [20]. The structure was modeled using the Lagrangian-based finite element method while the fluid was modeled using the Eulerian-based finite volume method. The structure is embedded into the fluid which is water in the present study. Two types of structural geometries were modeled inside fluid: a plate or a box-type structure.

2.1 PLATE MODEL

The first structural model is a plate in a towing tank. This model was developed to compare the numerical solution to the experimental data so as to validate the model. In the physical test, the plate was towed inside the towing tank containing water. However, in the numerical model, the plate is stationary in the towing tank and fluid flows around the plate. The relative speed is the same between the experimental and numerical studies. Figure 1 shows the plate with an attached bar in a towing tank. The bar is a part of the towing tank carriage assembly in order to move the plate in the towing tank for the physical experiment. The largest outside box in Fig. 1 indicates the water surrounding the structure, i.e., the towing tank. Other lines in the figure are just reference lines for the mesh generation purpose.

The plate has the dimensions of 328 mm long, 177.5 mm high and 3 mm thick. It is comprised of quasi-isotropic, 10 layers of E-glass woven composites with the density of 2000 Kg/m^3 and elastic modulus of 20 GPa, and is rigidly attached to the tow tank carriage assembly bar made of aluminum with dimensions of 26 mm × 26 mm cross-section and 2,178 mm long. The length of the aluminum bar secured to the plate is 77 mm as shown in Fig. 2. The finite element mesh of the plate and the supporting bar is also shown in Fig. 2. The mesh consists of 3-D brick-shape elements with 2,844 nodes and 14,759 elements. Several elements were used through the thickness of the plate in order to represent the bending behavior of the plate. Because fluid is in contact with both sides of the plate, shell elements could not be used to represent the plate. Shell elements do not have thickness in the geometric model so that fluid on both sides of the plate cannot be easily modeled.

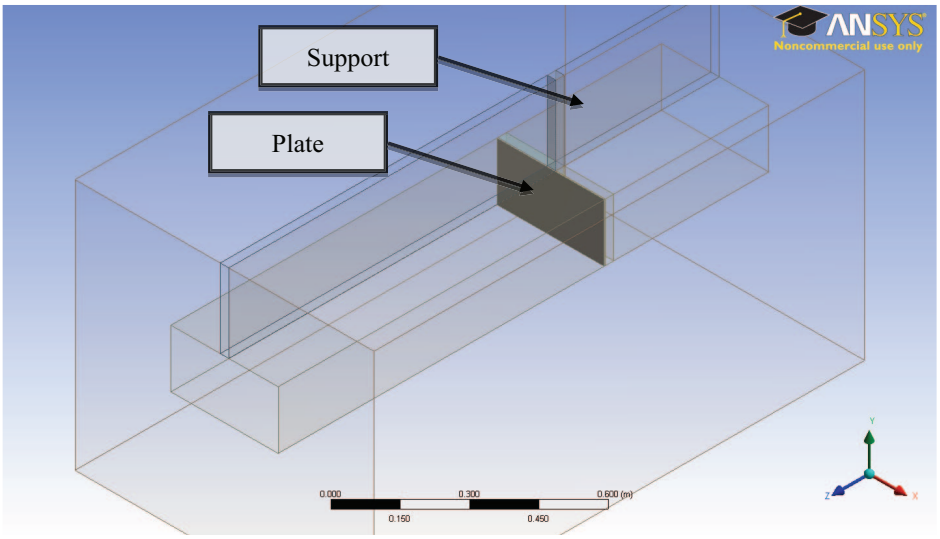

Figure 1: Plate supported by a bar inside a towing tank

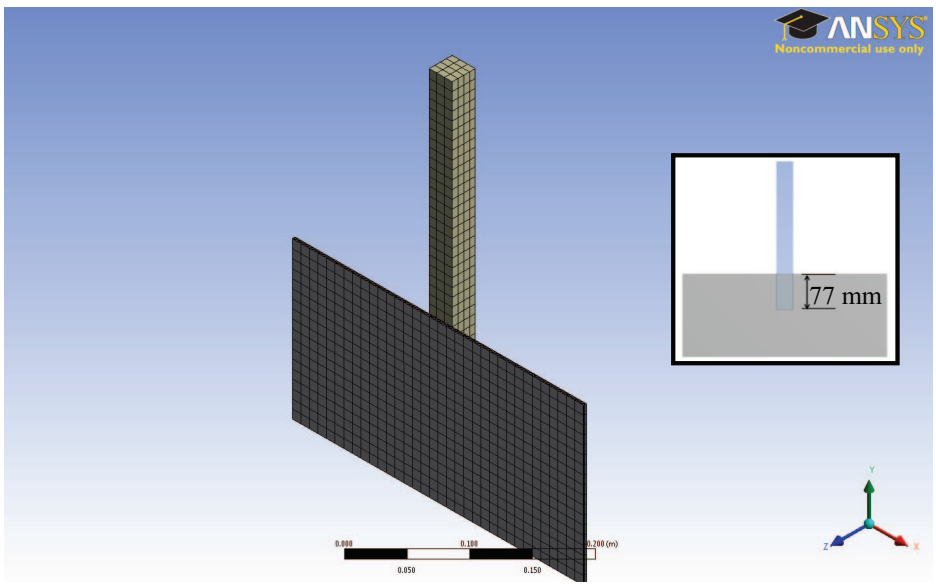

Figure 2: Structural mesh of composite plate and supporting aluminum bar

The towing tank was modeled as a rectangular box of the size of 0.914 m × 0.914 m × 2 m long. The fluid mesh has 83,893 nodes and 45,220 3-D brick shape elements. A study of mesh sensitivity was conducted and the present meshes were selected in terms of the solution accuracy and the computational efficiency.

As boundary conditions, the aluminum bar was fixed at the top to hold the plate in place while a uniform fluid velocity was applied to the towing tank inlet, the front face in Fig. 3. The inlet velocity was changed from 0 m/s to 0.5 m/s during 0.05 sec. with a constant

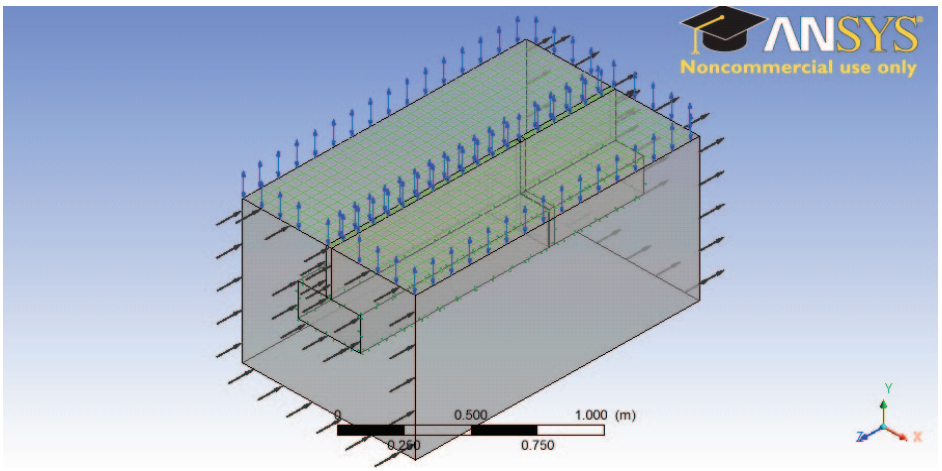

Figure 3: Fluid domain

acceleration to best represent the physical experiment. The towing tank outlet had a constant pressure, the two sides and the bottom face had no-slip flow boundary condition, and the top surface has a zero pressure boundary condition like a free water surface in the towing tank. Surely, the interface between the fluid and structure were also identified in the coupled model for fluid-structure interaction.

2.2 BOX MODEL

Because the experimental facility available at the laboratory is limited to s small scale and low velocity object, numerical studies were conducted for more diverse cases after validation of the computer model using the plate structure. For the numerical study, a box-shape structure was modeled for parametric studies. The solid object used in the base model was a 1 m^3 box created using shell elements. The structural mesh consists of quadrilateral shell elements with 3,458 nodes and 3,456 elements as shown in Fig. 4. The box-shape structure was varied later in terms of the shape and size for a series of parametric studies. However, the element size was remained relatively constant for different cases. The front surface was the same E-glass composite structure as before, which interacts with water while the other five sides were assumed to be rigid and fixed in space.

The fluid domain was sized sufficiently to ensure the development of the complete inlet velocity profile and to minimize interference from remaining sides of the fluid domain. The fluid domain extended one meter beyond the cube from its top, sides and the rear face; and two meters from the front face. The structure was surrounded by water on its outside. The fluid domain has the dimensions of 3 m × 3 m × 4 m. There is no fluid inside the box. The fluid domains had 110,937 nodes and 100,744 elements as sketched in Fig. 5. The water is assumed to have the density of 1000 Kg/m^3 and the kinematic viscosity of $1{,}0 \times 10^{-6}$ m^2/s. The Reynolds number for the base model of the box structure is 2×10^6.

The interfaces between the structure and fluid are defined as below. The front interface has the fluid-structure interaction. The other five sides of interface had no-slip boundary conditions since the structural parts were held fixed in space. The inlet side of the fluid domain had a prescribed velocity as a function of time. The outlet of the fluid domain had a prescribed constant pressure. Full-slip boundary conditions were also applied to all other

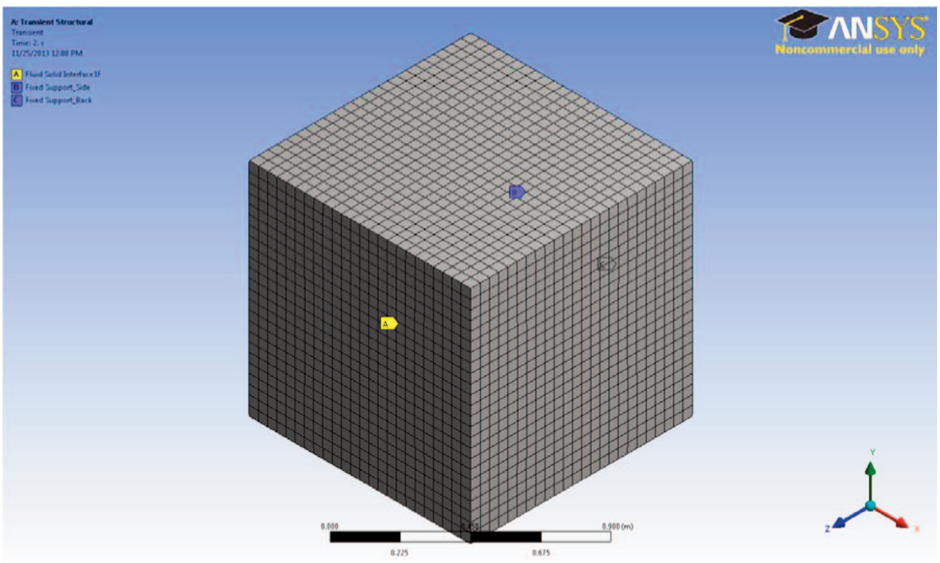

Figure 4: Mesh of a box-like structure

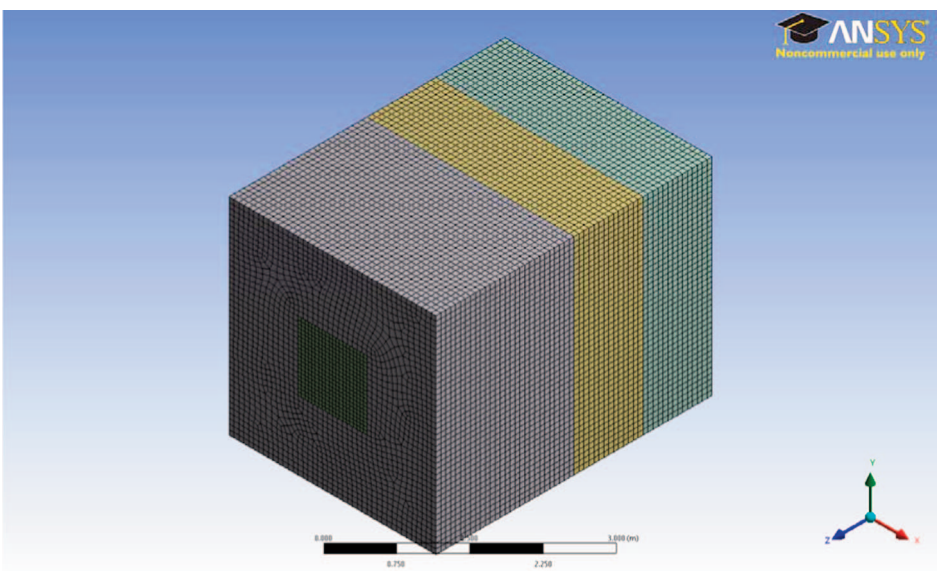

Figure 5: Mesh of fluid domain

exterior surfaces of the fluid domain in order to mitigate boundary layer effects from the fluid domain onto the cubic structure.

The description in the previous paragraphs is for the basic model. When there is any change in the base model as a parametric study, such a change is described in each case study. The change includes structural size, shape, material properties, fluid boundary condition, etc.

3. VERIFICATION OF COMPUTER MODEL

Experiments were conducted in a towing tank located at Naval Postgraduate School. The tow tank is 0.914 m wide, 1.52 m high and 11.6 m long. The tank was filled with water with 0.914 m high. A five horsepower motor pulls a carriage along the top of the tank to move the mounted plate to a specified speed. The E-glass composite plate was attached to the towing tank carriage assembly using bolts and nuts. The top side of the plate placed approximately 0.25 m below from the free surface of water. A load cell affixed to the tow cable measures the forces induced by the drag of the plate. The plate was pulled from rest to a steady state velocity of 0.5 m/s. The duration of speed change was 0.05 sec as measured by a high speed camera.

In order to measure the fluid force on the composite plate, two tests were conducted. The first test was conducted with water in the towing tank, and the second test was conducted without water in the towing tank. The force from the latter test was subtracted from the force from the former test. The purpose of the second test was to determine how much force is associated with pulling the towing tank carriage assembly system. The test without water was conducted with and without the composite plate. There was no noticeable difference between the two cases. As a result, the net fluid force on the composite structure was obtained.

The numerical analysis was conducted for the model described in the previous section, and the result is plotted in Fig. 6. The comparison of the results between the experimental and numerical studies is given in Table 1 which shows the peak as well as steady state fluid forces applied to the composite structure. The difference between the experimental and numerical study is about 20% and 10% for the peak and steady state forces, respectively. Such a difference results from some discrepancies between the physical experiment and numerical studies. During the physical experiment, it was observed that the free water surface on the top side of the towing tank fluctuated up and down like a wave motion as the plate moved.

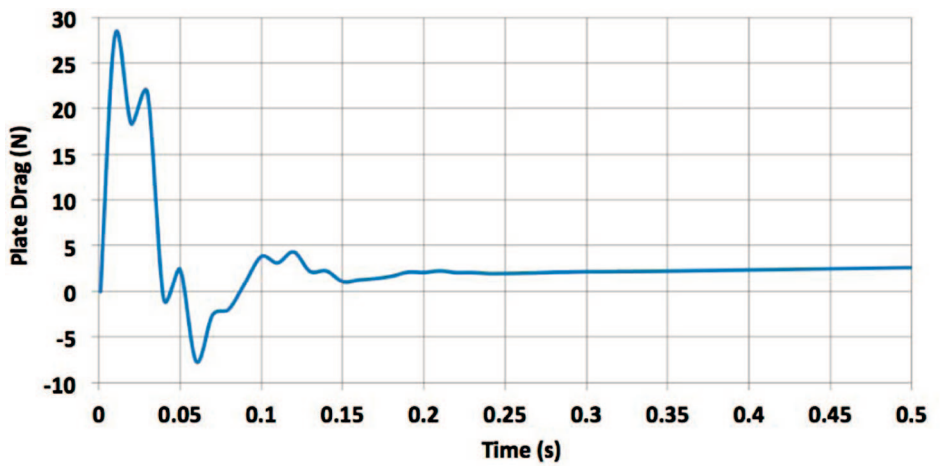

Figure 6: Fluid force on composite plate during physical experiment

Table 1: Comparison of fluid forces between numerical and experimental studies

	Max. transient force (N)	Steady state force (N)
Numerical Model	28.0	5.4
Experimental Model	34.2	4.9
Error	–22%	10%

However, the computational model did not include such a wave motion with the zero pressure boundary at the top. The high speed camera showed that the velocity change from the rest to the steady state velocity was not quire linear. There were some oscillations. Therefore, there is a difference between the constant acceleration in model and the physical acceleration. This certainly resulted in more discrepancy between the experimental and numerical data for the maximum transient force. Considering these discrepancies between the numerical and experimental studies, the numerical model yielded acceptable solutions. Then, the next box-like model was developed and analyzed numerically.

4. DESCRIPTION OF CASE STUDIES

Multiple cases were studied in order to determine the effect of the transient fluid force onto flexible composite structures. The basic geometric models of the structure and the surrounding fluid as well as the boundary conditions were described in a previous section. This section presents each case for the parametric study.

4.1 BASE MODEL: CONSTANT ACCELERATION FOR 0.5 SECOND

To facilitate proper evaluation for a diverse spectrum of transient flow conditions and geometric variants, a base model was selected and analyzed. The base model was described in a previous section. The base model considered transient fluid flow at the inlet under a constant acceleration for the first 0.5 sec. until a terminal velocity of 2 m/s was reached at which point the fluid velocity remained constant for the duration of the simulation as sketched in Fig. 7. A time step size of 0.01 seconds was used for plotting the results even though the actual time step size used for computation was much smaller.

4.2 VARIATION IN MAGNITUDE OF CONSTANT ACCELERATION

The inlet velocity profile used in the base model was formulated from the equation $y = 4x$ for 0.5 sec. As the first parametric study, it was necessary to establish the effects of different fluid accelerations on the composite material. Two cases were selected that increased and decreased the acceleration magnitude by a factor of two. The first case, 2 m/s at 0.25 sec, represented a flow that was twice as fast as the base model. This was achieved by

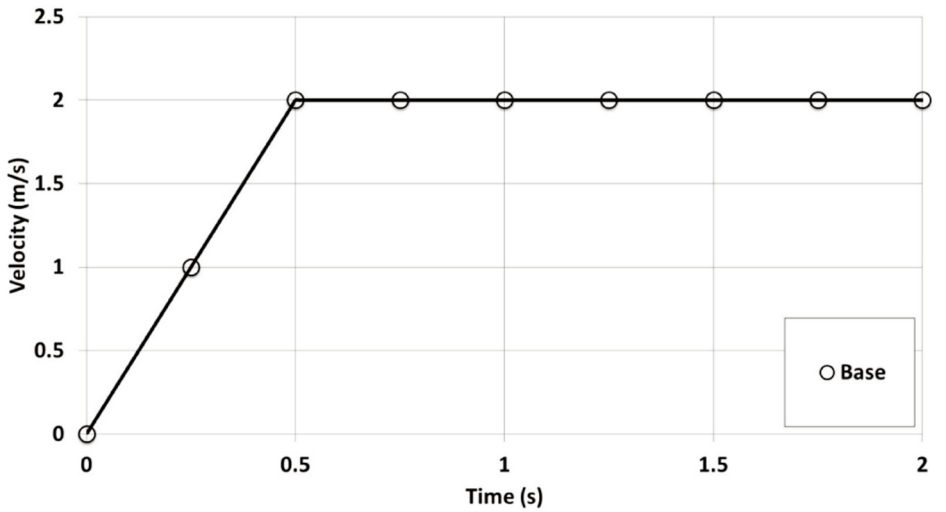

Figure 7: Inlet velocity profile of the base model

determining an inlet velocity profile from the equation y = 8x evaluated for 0.25 sec. until a maximum steady state speed of 2 m/s was achieved. The second case, 2 m/s at 1 second, was half as fast the base and modeled from the equation y = 2x evaluated for 1 sec. until a maximum steady state speed of 2 m/s. Figure 8 displays the inlet velocity profile for both acceleration variants and the base model.

4.3 VARIATION IN TERMINAL VELOCITY

Having simulated changes in acceleration, the next step in the study was to determine the effects of changes in terminal velocity. Using a similar approach to the one in the previous section, two cases were modeled that simulated terminal velocities higher and lower than the base model utilizing the same inlet acceleration equation of y = 4x. The first case extended the acceleration domain to 0.63 sec. and a terminal velocity of 2.5 m/s. The second narrowed the acceleration domain to 0.38 sec. and a resulted in a terminal velocity of 1.5 m/s; both terminal velocity and base model profiles are shown in Fig. 9.

4.4 STEP ACCELERATION

The step acceleration represents interruption in constant acceleration while the steady state velocities are the same as well as the durations of the total transient phase are also the same. This prompted the structural domain to respond to incremental increases in velocity and be subject to shorter periods of constant acceleration. The first case, called 4-step, simulated four periods of constant velocity at 0.5, 1, 1.5 and 2 m/s while the second case, 2-step, held velocity constant at 1 and 2 m/s. In both cases the mid-step acceleration was constant. Figure 10 shows both 4-step and 2-step inlet velocity profiles compared to the base model. Although all simulations completed the full two seconds, only the transient portion is shown in the figure.

4.5 MONOTONICALLY VARYING ACCELERATION

Real world acceleration is rarely constant and thus the next cases represented an inlet velocity profile similar to that of a ship accelerating from rest. The first case modeled a monotonically increasing acceleration and the second was monotonically decreasing as shown in Fig. 11. Together they show the effects of nonlinear acceleration during the period

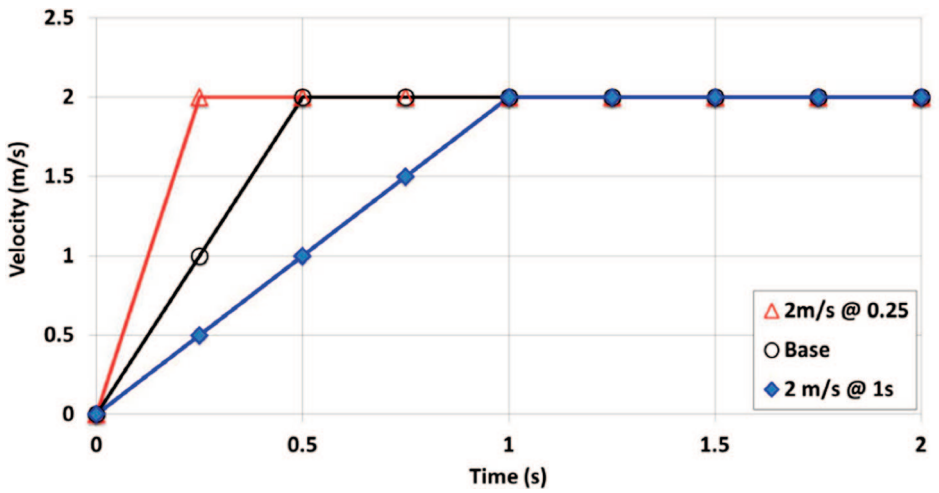

Figure 8: Inlet velocity profiles of variation in constant acceleration

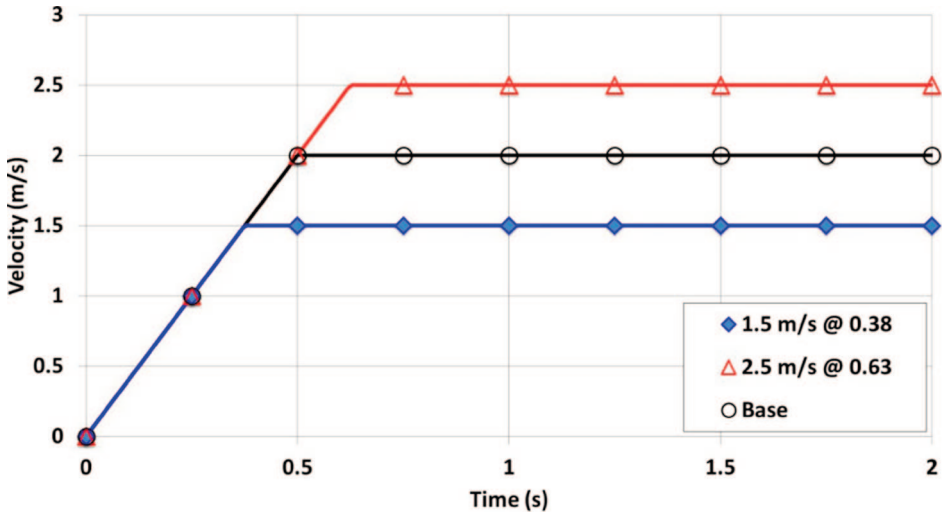

Figure 9: Inlet velocity profiles of variation in terminal velocity

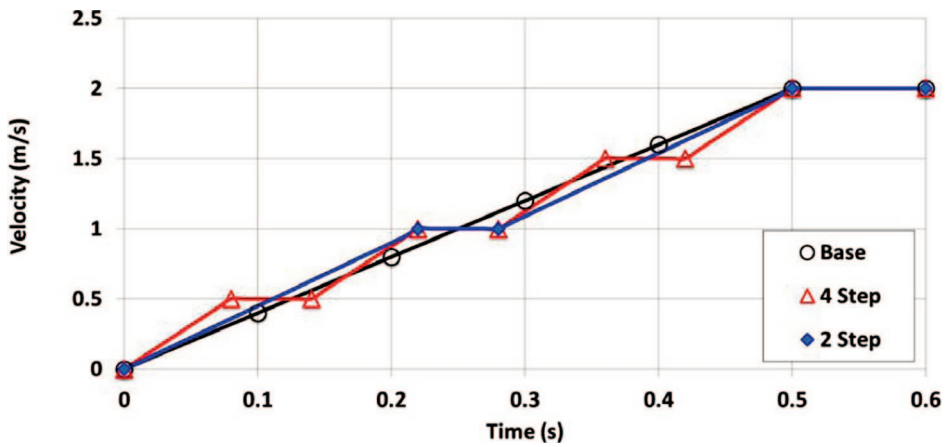

Figure 10: Inlet velocity profiles of step accelerations

of velocity variation. Both simulations completed the 2-second run although only the pertinent sections are shown in Fig. 11.

4.6 GEOMETRIC VARIATION

The next study examined the effect of structural geometry changes on structural responses. While flat plates in flow are useful for a basic study, far more complex geometry is easily expected in ship design. Therefore, it was important to gain an understanding of how changes in geometry would affect the stresses induced by the flow.

The first geometry variant was a reduction in cube size by half, from one meter to 0.5 meter on all sides. The next geometric shift was the transition from a cube to a cylinder. In this case a flat-faced one-meter diameter cylinder replaced the cube as seen in Fig. 12. The final geometric variant replaced the flat font surface of the cylinder with a semi-spherical dome of 1 m diameter.

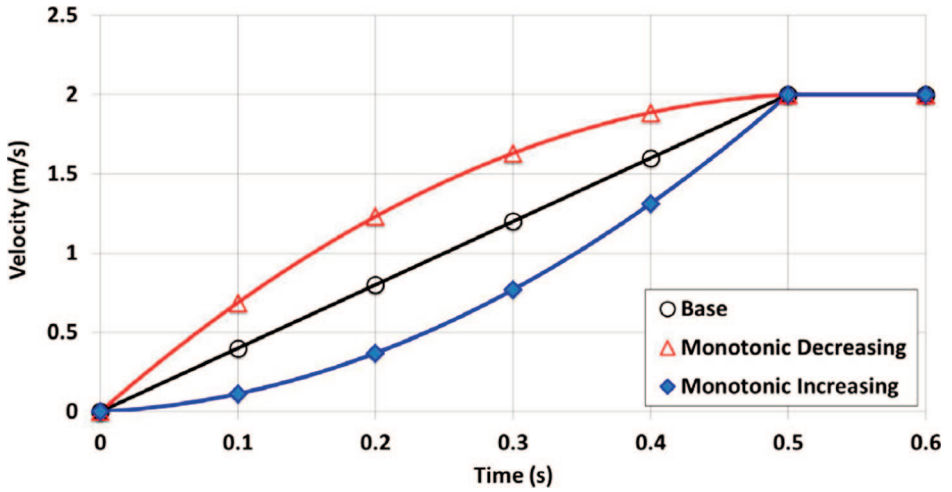

Figure 11: Inlet velocity profiles of monotonically varying accelerations

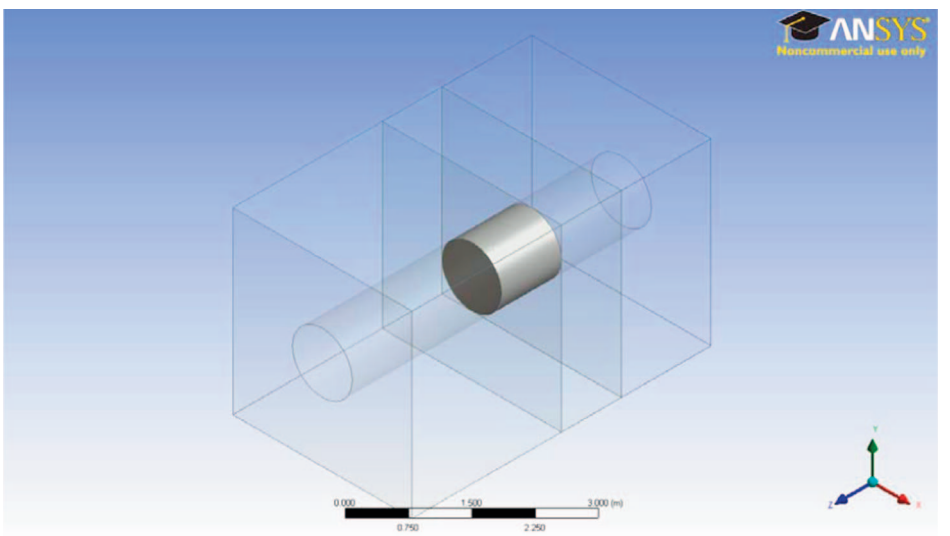

Figure 12: Cylinder with flat front face

4.7 VARIATION IN MATERIAL PROPERTY

The final cases varied material properties of the base model. By changing the density and Young's modulus, an evaluation of their effects on structural responses to an accelerating fluid was obtained. There were no additional changes made from the base model to include inlet velocity profile. Material properties for these three models are presented in Table 2.

4.8 VARIATION IN WATER DEPTH FROM FREE SURFACE

Having completed the full range of inlet velocity changes, it was necessary to add another variable for comparison, which would be considered as another element of ship design. The boundary conditions used in the base model represent a submerged cube in an infinitely large

Table 2: Variation in Material Property

	Base	2000/50	2000/100	3000/50
Density (kg/m3)	2,000	2,000	2,000	3,000
Young's modulus (GPa)	20	50	100	50

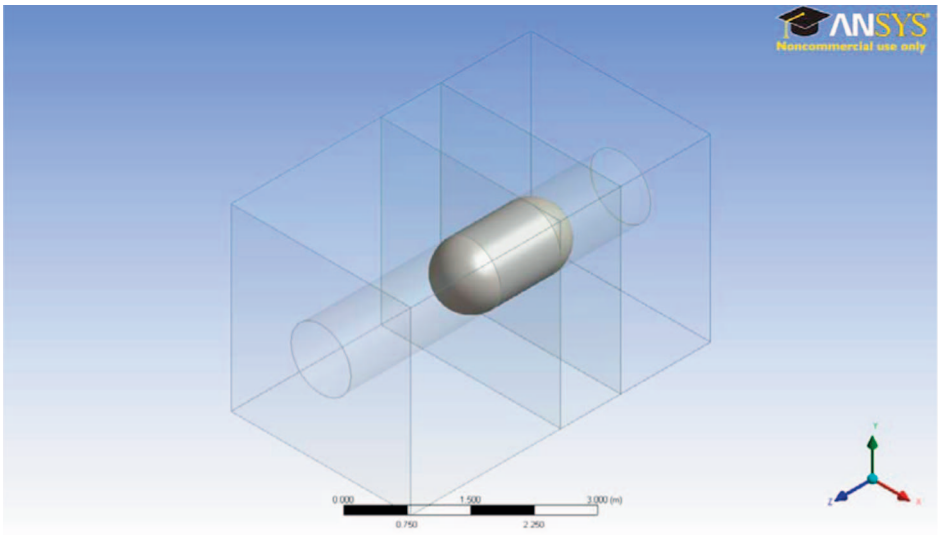

Figure 13: Cylinder with dome-shape front face

fluid domain, similar to an underwater vehicle, in which there is no boundary effect on all sides. To enable application to surface vessels, a free water surface was modeled by configuring the upper fluid boundary with zero pressure. All depth simulations included the free water surface and retained the same inlet velocity profile as the base model.

The first depth case, set at one meter, was identical to the base model with the only change being the addition of a free surface. This allowed for a direct comparison to depict the effects of the free surface. The second and third cases increased the depth to two and three meters, respectively.

5. RESULTS

5.1 BASE MODEL

The base model consisted of a one-meter cube fully submerged in fluid domain with the front face of the cube allowed for FSI as exposed to fluid flow. The inlet velocity profile shown in Fig. 7 was applied to the base model. As the first study, the flexible front plate of the base model was changed into a rigid plate so that there was no FSI. Then, the two models with and without FSI were compared to examine the effect of FSI on the fluid flow.

After completing simulations for both models, the center node of the flexible base model has the maximum 45 mm inward displacement at 0.09 sec., the maximum 15 mm outward displacement at 0.58 sec., and the steady state 5 mm inward displacement at 2.0 sec. These local maximum/minimum and steady state displacement should have the largest effect on fluid flow around the cube. The responses at those time steps (i.e., 0.09, 0.58 and 2.0 sec) are compared between the flexible and rigid plates in Figs. 14–19.

At the time of 0.09 sec., the inward deflection of the deformable plate minimizes overall resistance on the upstream flow field and allows upstream fluid to progress at a faster average velocity than the rigid model. The velocity contours at 0.09 sec. are compared between the two models in Figs. 14 and 15. The velocity contours around the front plates are quite different between the two models because of the effect of FSI.

The maximum outward deflection of the flexible plate occurred at 0.58 sec. and gave the cube a slight streamline effect that resulted in an average velocity around the cube of 2.32 m/s.

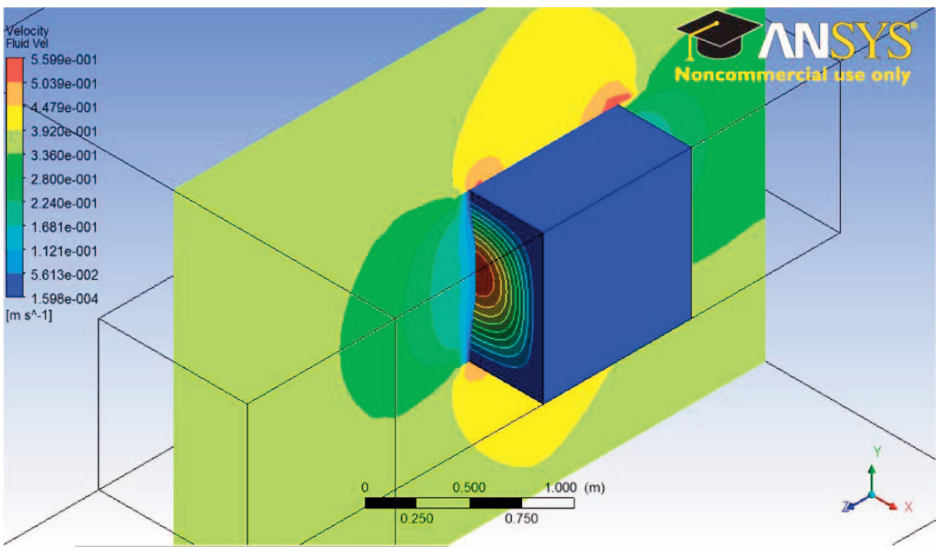

Figure 14: Plot of fluid velocity contour and plate deformation for the flexible base model at 0.09 sec.

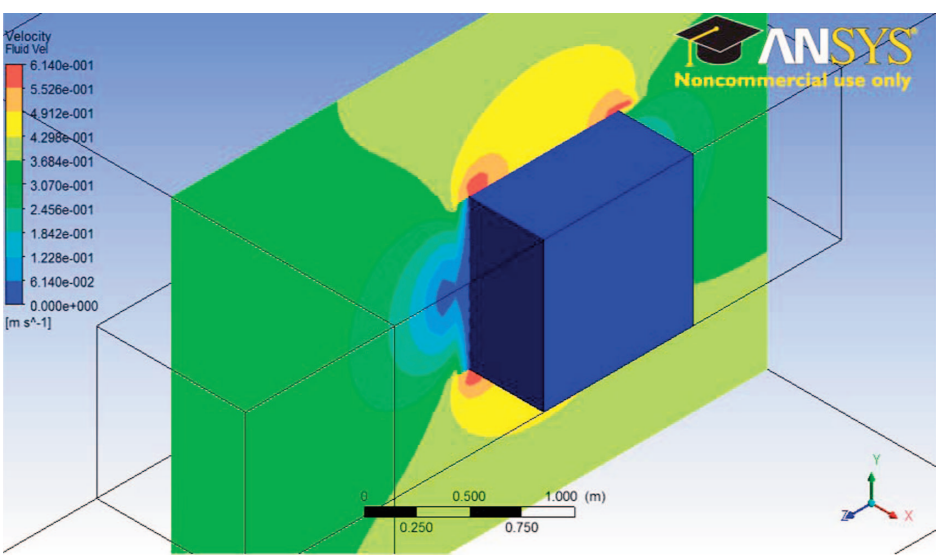

Figure 15: Plot of fluid velocity contour for the rigid base model at 0.09 sec.

The average fluid velocity of the rigid body around the cube at 0.58 sec. was 2.22 m/s and slower than the flexible model. Figures 16 and 17 compare the velocity contours at 0.58 sec. The difference in velocity contours of the two models is less with the maximum outward deflection at 0.58 sec. than with the maximum inward deflection at 0.09 sec. The velocity contours between the two models at the steady state (i.e., at 2.0 sec.) are virtually identical with only minor velocity differences of approximately 0.002 m/s, as compared in Figs. 18 and 19.

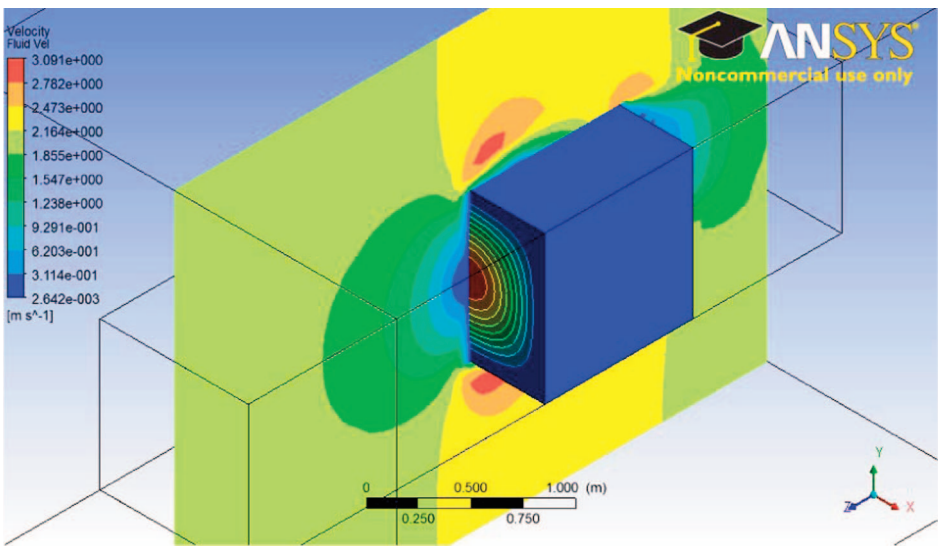

Figure 16: Plot of fluid velocity contour and plate deformation for the flexible base model at 0.58 sec.

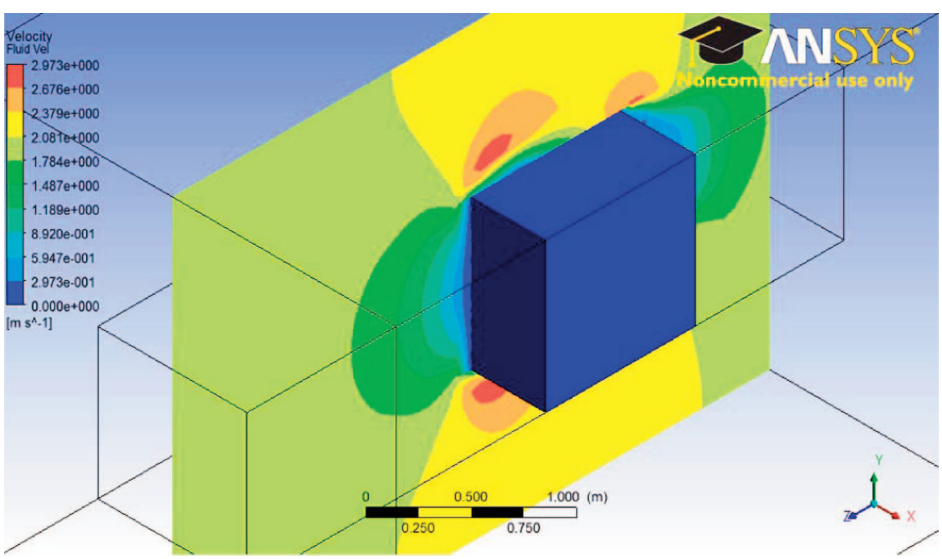

Figure 17: Plot of fluid velocity contour for the rigid base model at 0.58 sec.

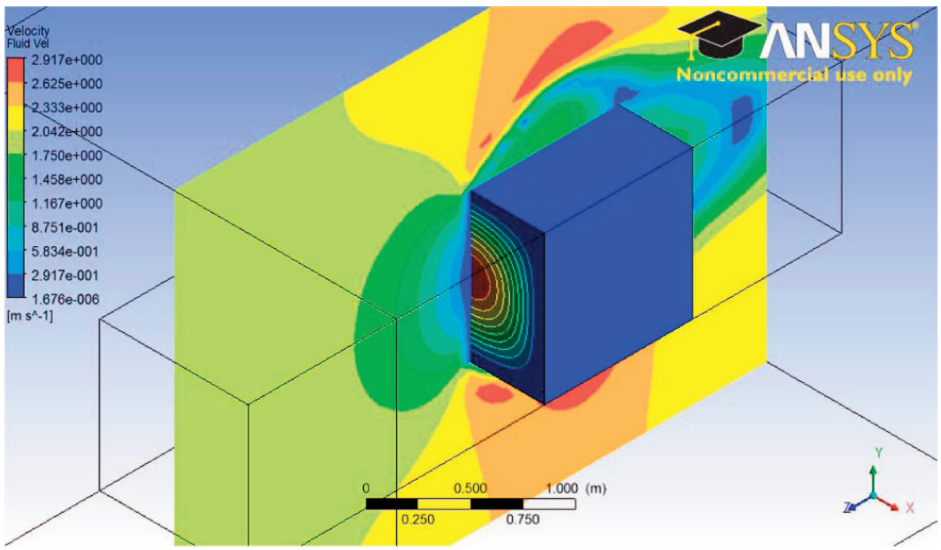

Figure 18: Plot of fluid velocity contour and plate deformation for the flexible base model at 2.0 sec.

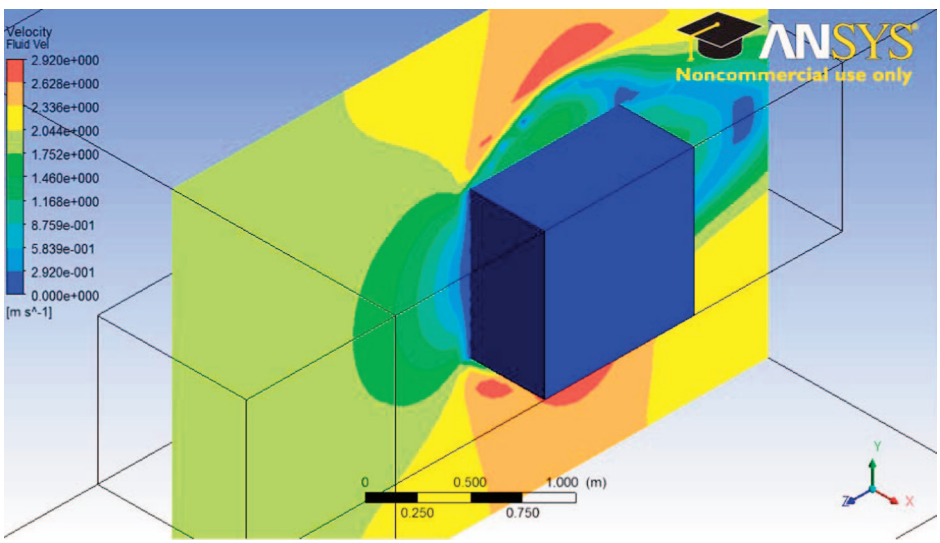

Figure 19: Plot of fluid velocity contour for the rigid base model at 2.0 sec.

Once the effect of FSI was studied using the base model, the flexible base model was further analyzed to investigate the effect of the transient flow on the flexible front plate. From now on, the base model refers to the box with the flexible front plate. In order to determine the maximum stress/strain in the structural domain caused by transient flow, it is necessary to first verify the location of peak stress or strain. By checking the computer results, it was found the maximum stress/strain occurs near the clamped boundaries. Figure 20 shows a representative equivalent strain contour in the plate. The elastic equivalent strain is

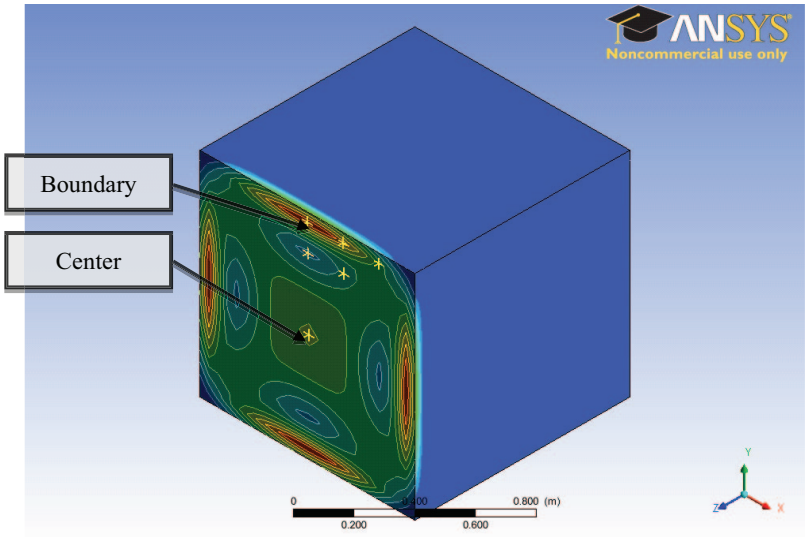

Figure 20: Plot of flow velocity contour for the rigid base model at 2.0 sec.

like the von Mises stress in terms of strain components. One of the maximum strain locations was picked and called the "boundary point" from now on. Figure 21 compares the elastic equivalent strains at the boundary point and the center as a function of time. This plot shows that the boundary point has much highest strain value than at the center. This is because of the clamped boundary.

The ratio of the maximum transient value to the steady state value of the elastic equivalent strain is a little over than eight at both the center and the upper nodes. This ratio remained the same for the von Mises stress as well as the maximum displacement, as expected. Furthermore, nodal acceleration and displacement at the center are plotted in Fig. 22.

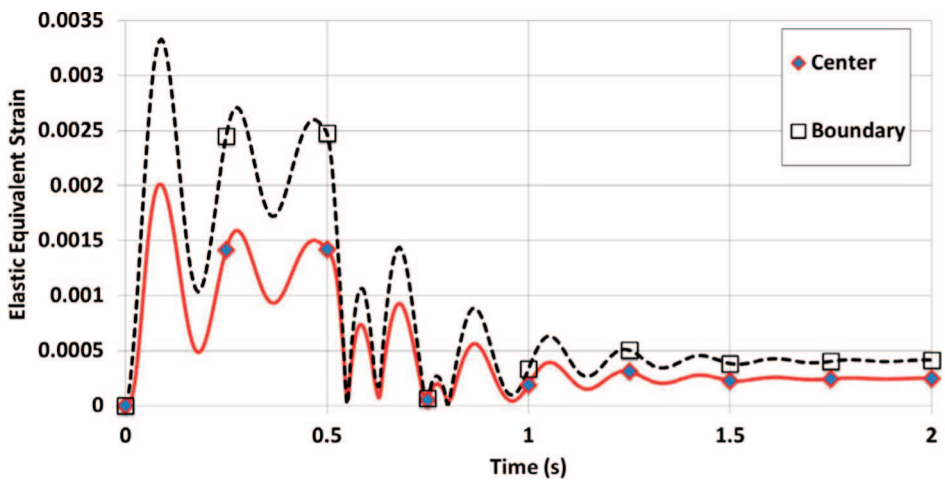

Figure 21: Plot of time history of elastic equivalent strain at two locations of the front plate of the base model

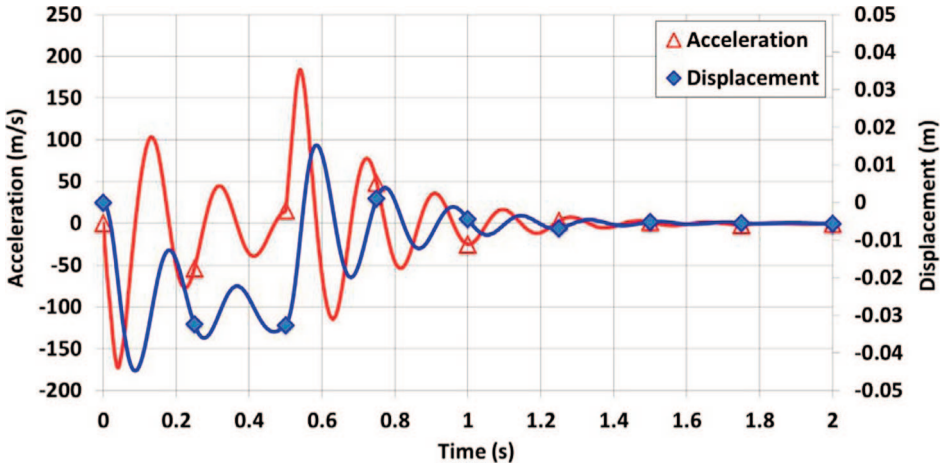

Figure 22: Plot of time history of acceleration and displacement at the center of the base model

Plate displacement corresponded closely to acceleration with expected minimal lag between the two variables. There was an average 0.04 sec delay of the local maximum and minimum displacement values to acceleration values. Peak values for structural stress and strain occur during times when displacement is at either a local maximum or minimum. Lastly, at 0.5 sec., the fluid acceleration suddenly changes to zero as shown in Fig. 7, and there was an immediate response in structural nodal acceleration as well as in displacement.

Fluid pressure at the center of the plate was the final data point evaluated from the base model. Additionally, the average fluid pressure over the entire flexible plate was also computed and plotted in Fig. 23. Multiplication of the average pressure by the plate surface area results in the total fluid force on the plate. The average pressure plot closely matched the pressure plot at the center node. The ratio of the maximum to the steady state values was also computed for the two kinds of fluid pressure, i.e., pressure at the plate center and the

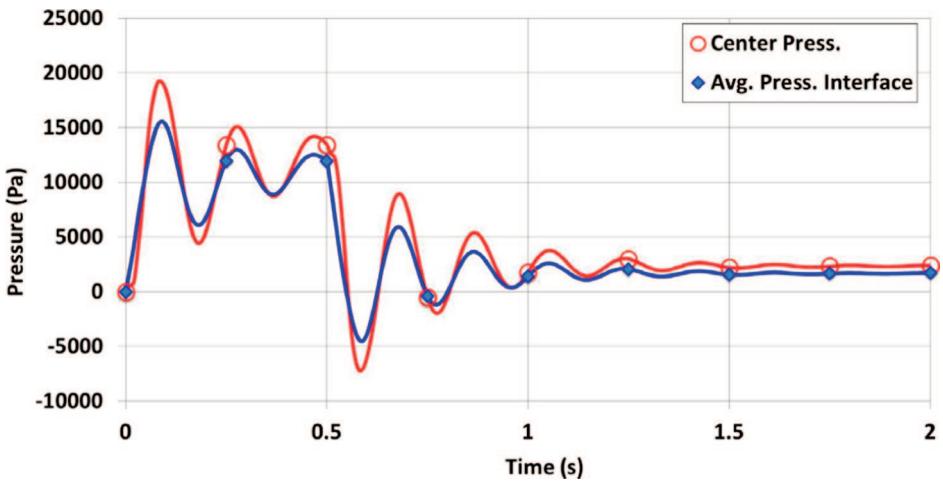

Figure 23: Plot of fluid pressure at center and average fluid pressure over the entire plate of the base model

average pressure. The ratio for the fluid pressure at the plate center was very close to that obtained for the stress and strain values, i.e., a little over eight. However, the ratio for the average pressure was 14% greater than that for the central pressure.

One more thing to be noted here is that the negative pressure in Fig. 23 suggests potential local cavitation. However, such cavitation does not affect the initial maximum transient response before cavitation as well as the final steady state response long after cavitation. As a result, potential cavitation was not considered in this study.

5.2 VARIATION IN MAGNITUDE OF CONSTANT ACCELERATION

The cases evaluated here were the comparison of different magnitudes of constant acceleration models. The base model achieved a terminal velocity of 2.0 m/s at 0.5 sec. and the comparative models achieved the same speed in 0.25 sec. and 1.0 sec. Figure 24 compares the time history plots of von Mises stresses at the boundary point, i.e., the maximum stress location, for the different values of acceleration. The maximum stress was recorded at 0.09 sec. during the first inward oscillation of the interface regardless of the value of the constant acceleration, which correlated with the times for maximum displacement as expected.

The ratios of the transient maximum to steady state values of stress and strain are plotted against the magnitude of constant acceleration in Fig. 25. All three simulations evaluated in this case shared identical geometry and boundary conditions and the only variant was the magnitude of constant acceleration. This plot clearly shows a linear relationship between the magnitude of constant acceleration and the maximum to steady state ratio in stress/strain. This case indicates that the maximum stress is independent from terminal steady state velocity. If a structural design is based on terminal velocity without considering transient flow conditions, such a structure could fail.

Another observation was made regarding the oscillation in the stress plot of Fig, 24. Immediately after reaching the steady state velocity, the oscillation in the stress plot has a higher frequency for a while. The 2.0 m/s at 1.0 sec. model showed that the oscillation in the stress plot damped out before the steady state velocity was reached, and then new oscillation occurred with the sudden change in velocity at the beginning of the steady state velocity.

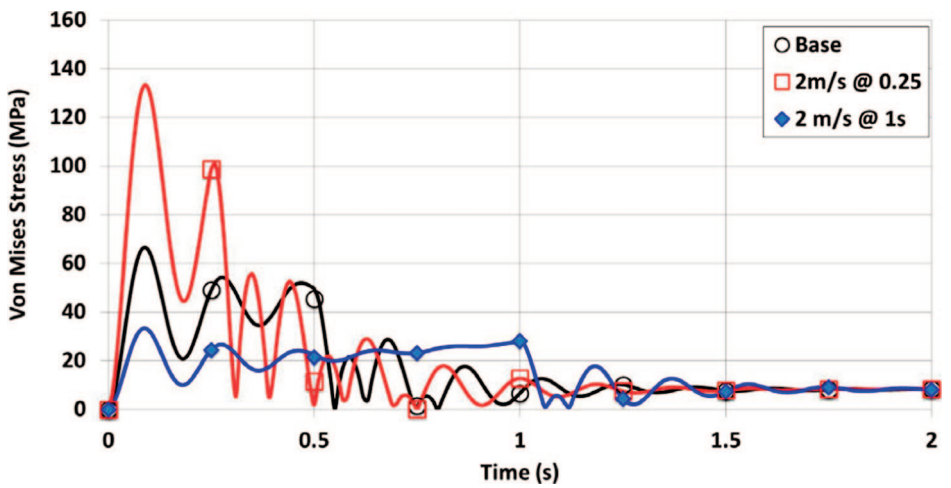

Figure 24: Plot of von Mises stress at boundary point for different magnitudes of constant acceleration

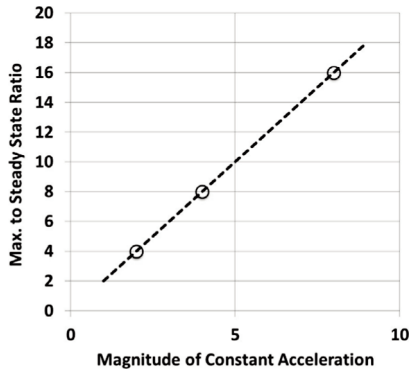

Figure 25: Plot of ratios of maximum to steady state stress/strain against magnitude of constant acceleration

5.3 VARIATION IN TERMINAL VELOCITY

The following cases evaluated the peak stresses induced by a change in terminal velocity. The base model reached a terminal velocity of 2 m/s and therefore suggested that simulations be run to terminal velocities of 2.5 m/s and 1.5 m/s. As expected, the peak stress and strain values were recorded at 0.09 seconds during the first maximum inward oscillation of the front plate. While the peak values were identical for all three cases, the steady state values differed due to the terminal velocity.

The ratio of the maximum to steady state values of stress/strain is plotted in Fig. 26 against the terminal steady state velocity. The ratio is inversely proportional to the terminal steady state velocity. The results from this case differed from the previous case in that the steady state value was the primary variable instead of varying magnitudes of the acceleration. Thus, the slower terminal velocity (and subsequent lowest steady state fluid pressure) had the highest ratios.

This case also gives additional insight into plate oscillation in response to the fluid force. As shown in Fig. 27, the initial displacement occurs in the negative direction and oscillations

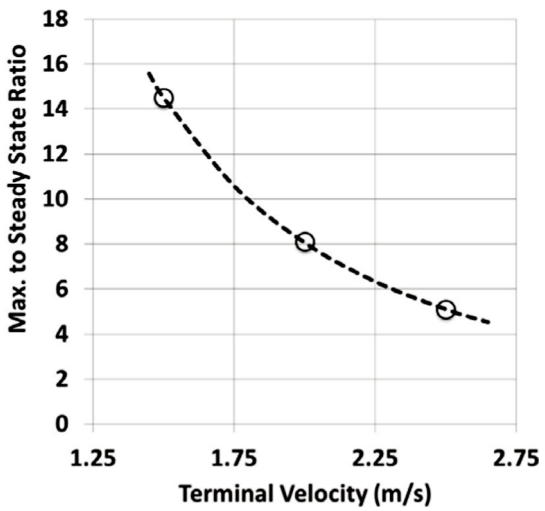

Figure 26: Plot of ratios of maximum to steady state stress/strain against terminal steady state velocity with the same constant acceleration

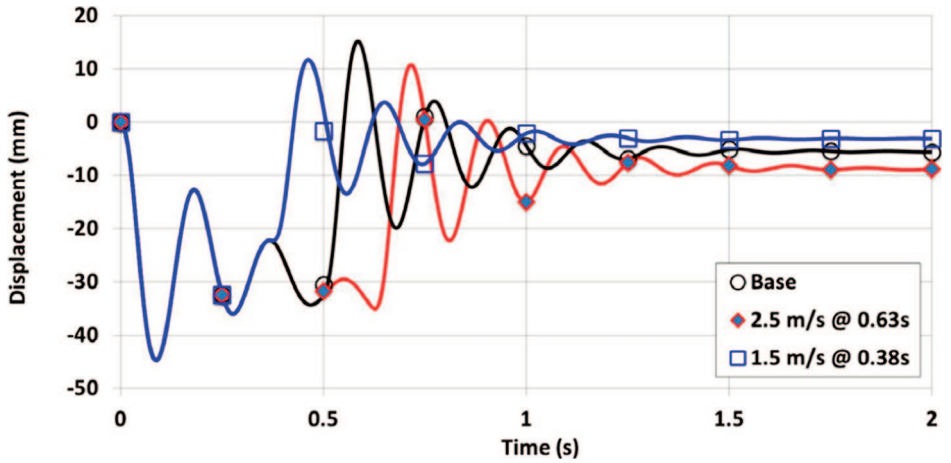

Figure 27: Plot of time history of displacement at the center for different terminal steady state velocities with the same constant acceleration

remain entirely negative until the steady state velocity reached. As soon as the velocity reached the steady state value, the plate moved toward a positive deflection, and its oscillation decayed to a constant steady state negative displacement.

5.4 STEP ACCELERATION

This case study examined the structural response resulting from interruptions in acceleration. The 4-step model had four periods of zero acceleration and the 2-step model had two while acceleration was held constant between steps. Because the final time to reach the same steady state velocity remains the same, the magnitude of acceleration is larger for the 4-step model as shown in Fig. 10. There were no changes made to the base geometric model.

The peak inward displacement occurred at different times for all three cases. While the base model peaked at 0.09 sec., the 4-step model peaked during the second zero acceleration period at 0.24 sec. and the 2-step model peaked halfway through the second acceleration period at 0.39 sec. The maximum von Mises stress at the boundary point coincided with the maximum deflection at the center.

These results indicate that successive interruptions in acceleration can have a serious effect on transient forces. The two-step model showed a 25% increase in the maximum stress while the four-step model increased the stress by 72%. Although acceleration was constant between the interruptions for each model, the three models did not share the same acceleration. The 4-step model had the highest acceleration of 6.25 m/s^2, the 2-step was second highest with 4.5 m/s^2 and the base model had an acceleration of 4 m/s^2. If there were no interruption in the acceleration, the acceleration of 6.25 m/s^2 in the 4-step model would have resulted in a 56% increase in the maximum stress instead of a 72% increase. The additional increase in stress was caused by the interruption. Likewise, the acceleration of 4.5 m/s^2 in the 2-step model would have resulted in a 13% increase in the maximum stress without interruptions. Although previous cases also indicated that peak transient stress occurred upon initial negative displacement, both 4-step and 2-step models had peak transient stresses that occurred during the second and third inward displacements respectively. This indicates that interruptions in acceleration have an effect on the peak transient stress.

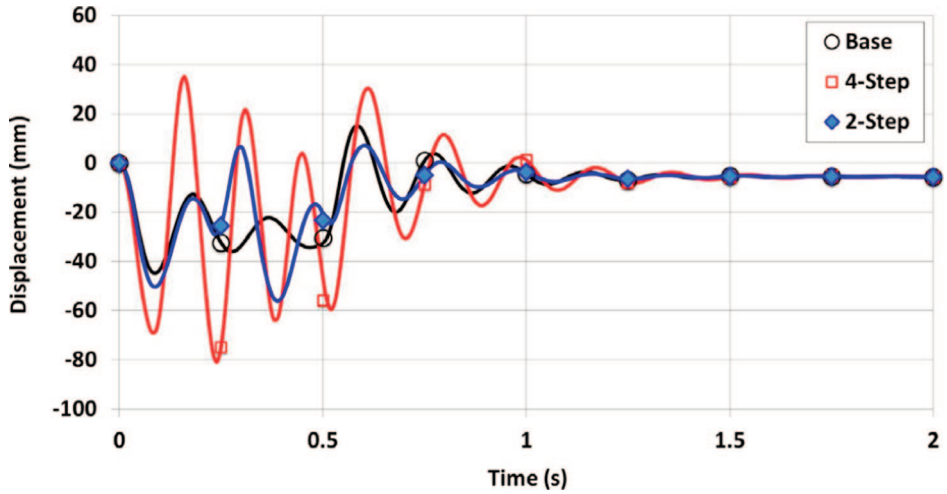

Figure 28: Plot of time history of displacement at the center for different step acceleration

Oscillatory responses of both 4-step and 2-step models showed unique results. For the 2-step model, zero acceleration periods began at 0.22 sec. and 0.5 sec., and both of these times correlate to sharp increases in plate displacement and sharp reductions in fluid pressure. The plate response in the 4-step model indicated sharp rises in stresses that correlate with the interruptions in acceleration at 0.08 sec., 0.22 sec., 0.36 sec. and 0.5 sec.

Figure 29 compares peak to steady state stress ratios to the common variable of acceleration interruptions. The base model was considered as one interruption while the 2-step and 4-step models had two and four interruptions, respectively. The plot in Fig. 29 is not a linear function as shown in Fig. 25. Such a deviation came from the multiple interruptions.

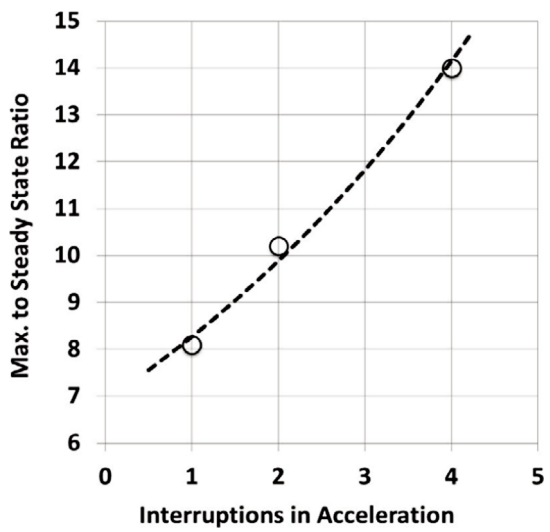

Figure 29: Plot of ratios of maximum to steady state stress/strain against no. of interruptions in acceleration

The stress ratios are larger with the multiple interruptions than those values calculated using the same magnitude of the acceleration without multiple interruptions.

5.5 MONOTONICALLY VARYING ACCELERATION

Monotonic changes in acceleration were investigated in this case as shown in Fig. 11. The monotonically increasing acceleration closely resembles the profile of an accelerating ship where acceleration increases with time. On the other hand, the monotonically decreasing model is a near mirror image.

As seen in Fig. 30, the monotonically decreasing model has a near-linear acceleration for the first 0.25 sec. and the plate responds with oscillations similar to the base model, which also has a linear acceleration. However, the monotonically decreasing model has a larger slope than the base model, which results in oscillations with a higher amplitude. During the final 0.25 sec. of the velocity transient, acceleration slowly reduces to zero in the monotonically decreasing model. This caused the oscillations to be reduced prior to achieving the steady state velocity so that the amplitude of stress became lower for the monotonically decreasing model than for the base model. On the other hand, the monotonic increasing simulation undergoes increasing acceleration that adds steadily increasing hydrodynamic forces and prevents the plate from an oscillatory response.

As Fig. 31 shows, the monotonically decreasing model had the largest ratio of peak to steady state stresses. This is expected based on the initial linearity of the fluid acceleration with a greater slope than the base model. The monotonically decreasing and base models reached peak displacements in the negative direction at 0.08 sec. and 0.09 sec. respectively. The monotonically increasing model reached a maximum inward displacement at 0.5 sec. and the ratio was higher than the base model because its slope was higher during the second half of the transient.

When a monotonically increasing acceleration is followed by a monotonically decreasing acceleration, such a combined velocity profile portrays a transient velocity curve with an inflection point and reduced acceleration slopes at both ends. This combination brings the advantages of each curve and avoids the initial transient oscillation while encouraging rapid oscillation decay prior to reaching steady state velocity. This type of transient velocity curve is also most representative of a ship at sea and proves that the attributes inherent to a transient acceleration are beneficial for the structure.

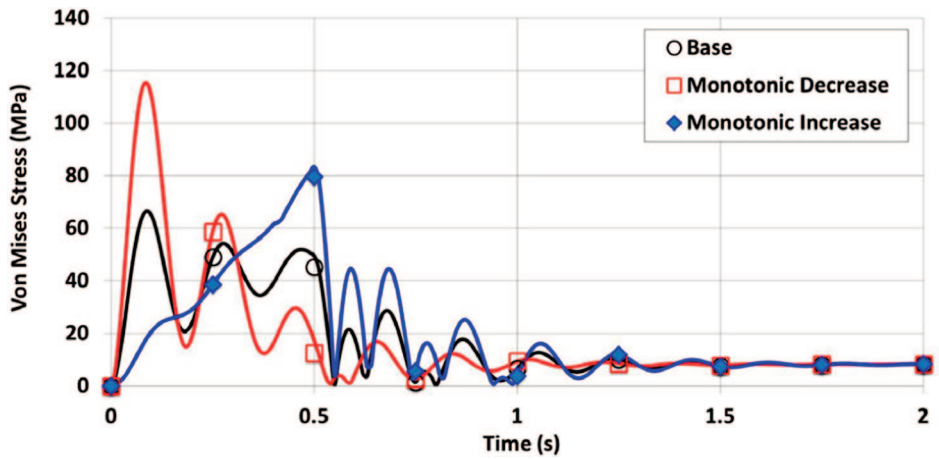

Figure 30: Plot of von Mises stress at boundary point for monotonically varying accelerations

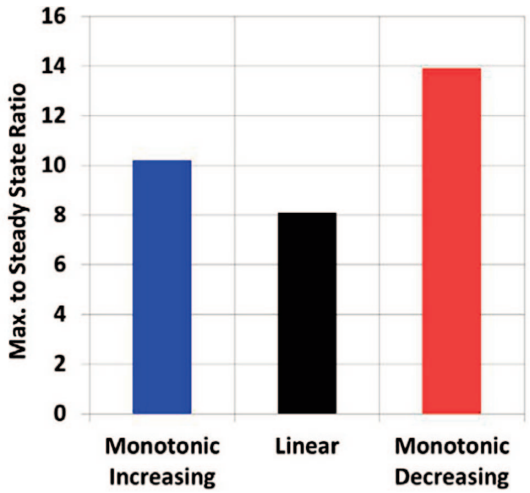

Figure 31: Plot of ratios of maximum to steady state stress/strain against monotonically varying acceleration

5.6 GEOMETRIC VARIATION

These cases investigate the effects of geometry on peak stresses. To maintain continuity, all cases were again compared to the base model and received the same inlet velocity profile, attaining 2 m/s at 0.5 sec. The first model was the cube sized down by one-half (called cube 0.5), the second was a flat face cylinder (called flat cylinder), and the third was a dome-faced cylinder (called dome cylinder). The geometric changes of this case required verification of the peak stress location. The peak stress locations for the cube 0.5 and flat cylinder models were near the boundaries like the base model. However, the dome cylinder model had a peak stress near the center of the dome.

Of the four models compared in this case, the base model experienced the highest peak stresses at approximately the same time as the flat cylinder model, and both models had also almost the same peak stresses. Although both models were one meter wide, the base model had a slightly larger surface area. Both models had similar oscillatory responses as occurred in the previous cases, as shown in Fig. 32.

The cube 0.5 model had significantly reduced stresses compared to the base model. The reduced size of the cube with the fixed boundary reduced the displacement compared to the base model. The cue 0.5 model had a less fluid pressure compared to the base model.

The last model under consideration was the one-meter diameter cylinder with a 0.5-meter radial dome on the front side. This geometry provided significantly lower stresses than anything evaluated in previous models. The curved dome adds structural rigidity and minimizes hydrodynamic forces. Oscillations were seen when plotted alone, but they are negligible in comparison to any of the other cases. The advantages of a curved surface cannot be understated with respect to structural integrity and its widespread use in naval and aeronautical applications is justified. The ratio of the maximum to steady-state stresses is compared in Table 3. The dome cylinder model has the smallest ratio, but the ratio is still near four. In other words, the maximum stress during the transient fluid loading is four times greater than the stress during the steady state fluid loading.

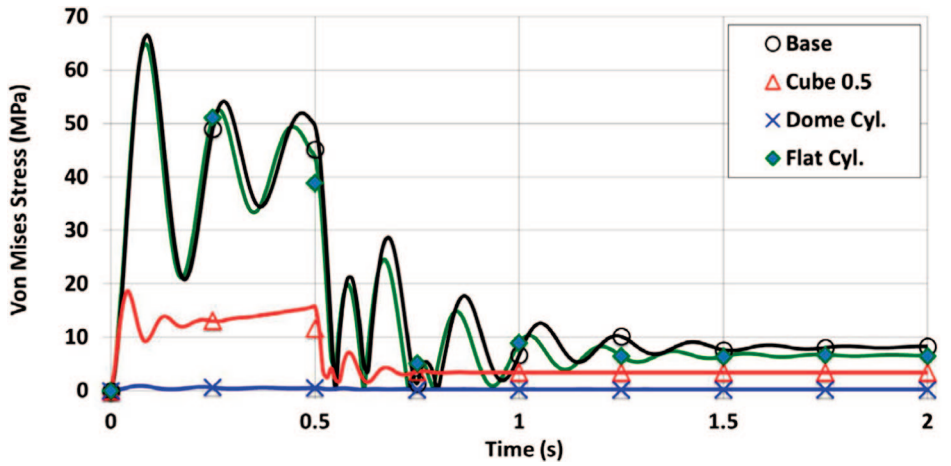

Figure 32: Plot of von Mises stress at their most critical locations for different geometric models

Table 3: Ratios of transient maximum to steady state stresses for different geometric models

	Dome cylinder	**Flat cylinder**	**Base cube**	**Cube 0.5**
Ratio	3.9	9.8	8.1	5.5

5.7 VARIATION ON MATERIAL PROPERTY

This case studied different composite materials subjected to the same boundary conditions and acceleration profile as the base model. The base model had a density of 2000 kg/m^3 and Young's modulus of 20 GPa, while the first and second models changed Young's modulus to 50 GPa and 100 GPa, respectively. The third model changed density to 3000 kg/m^3 and Young's modulus to 50 GPa.

Peak stresses for the base model occurred at 0.08 sec. while all others occurred at 0.07 sec. The base model has elastic modulus 20 GPa and density 2000 Kg/m^3. Thus, the three models (basic model, 2000Kg/m^3/50GPa model, 2000Kg/m^3/100GPa model) have the same mass density but different elastic moduli. Comparing the results shows the effect of the elastic modulus on structural strain and stress in Figs. 33 and 34. As expected, the lower modulus resulted in the higher strain as seen in Fig. 33. However, the resultant stress is higher with the higher modulus.

On the other hand, the two models (2000Kg/m^3/50GPa model, 3000Kg/m^3/50GPa model) can be compared to determine the effect of the mass density. The results indicated that the lower density yielded in the greater strain and stress. The lower density model showed approximately 15% higher stress than the higher density model. This suggests a lighter composite structure can have greater stress and strain under the same hydrodynamic loading, which should be considered in designs of marine composite structures. When the ratio of the maximum to steady state stresses are compared for all models, the base model had a slightly higher ratio than the other models. However, the difference is less than a couple percent so that it is negligible in the practical sense because material properties influenced both the transient peak stress/strain and the steady state stress/strain at almost the same proportion.

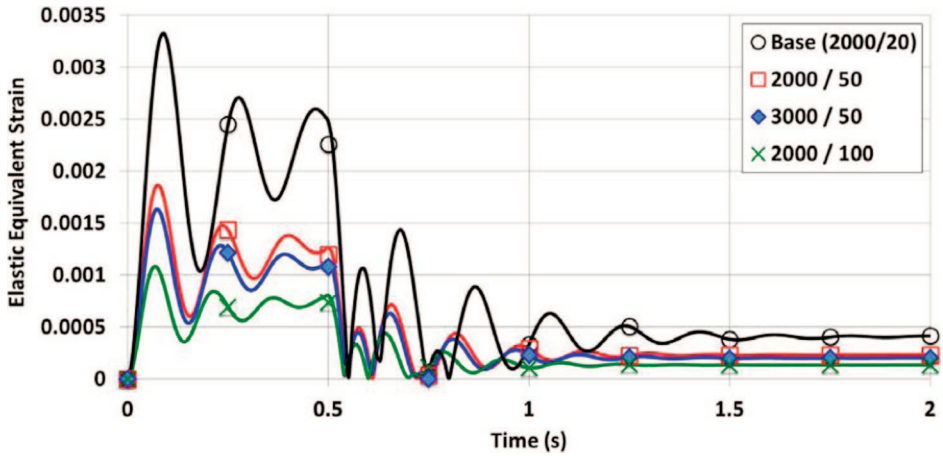

Figure 33: Plot of equivalent strain for different material properties

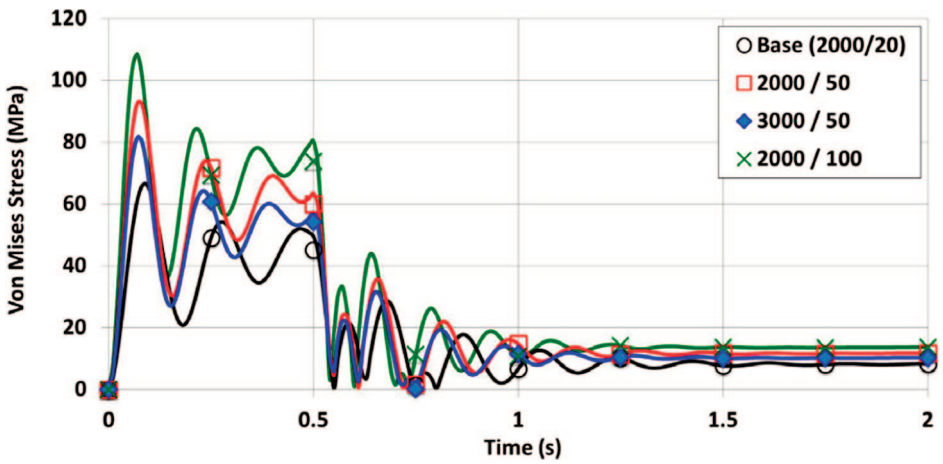

Figure 34: Plot of von Mises stress for different material properties

5.8 VARIATION IN WATER DEPTH FROM FREE SURFACE

The boundary condition applied to the top surface of the fluid domain was changed in this study. Previously, it was the free-slip boundary, but it was changed to the free boundary with zero pressure. Then, the structure was placed inside the fluid with the varying depth from the free surface. The *n*-meter model means the distance from the free surface of the fluid domain to the top surface of the structural box is *n* meter.

Although the time for peak pressure on the 1-meter model occurred at 0.07 sec. which is slightly earlier than that for the base model without the free fluid surface, the 1-meter model resulted in a far different response due to the significant effect of the free surface. Fluid along the upper half moved freely and resulted in much lower pressures above the cube. This also reduced the hydraulic forces applied to the fluid-structure interface as compared in Fig. 35 which shows the fluid pressure distribution on the vertical mid-plane around the cubic structure with two different boundary conditions at the top surface.

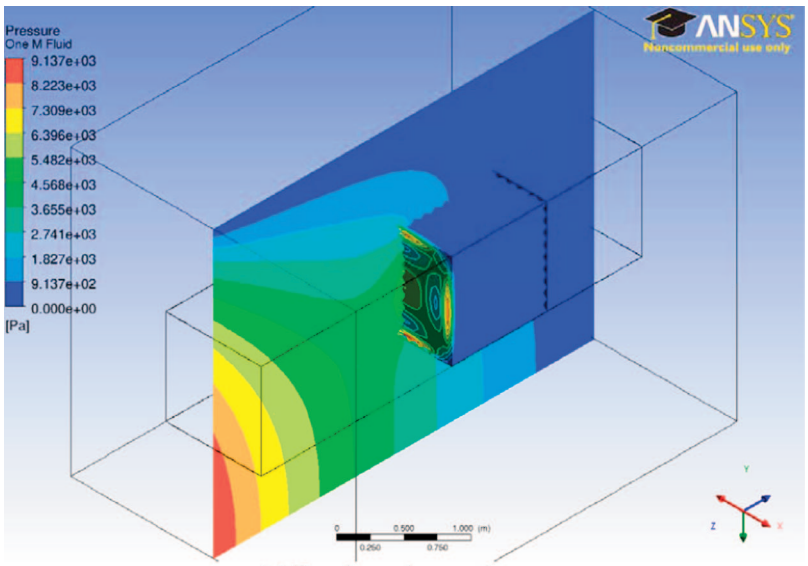

(a) Free boundary at the top

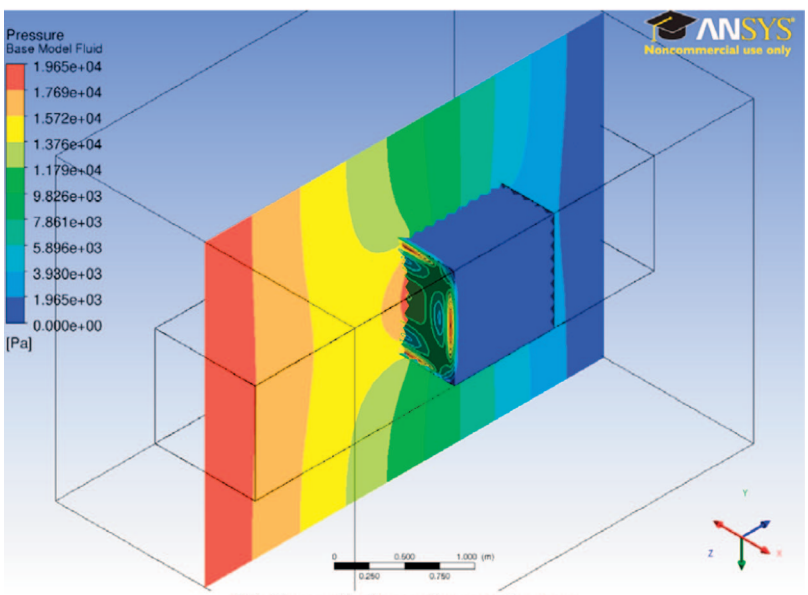

(b) Free-slip boundary at the top

Figure 35: Comparison of fluid pressure at the mid-surface of the fluid domain between two different boundary conditions at the top surface

The base model represents an infinite water depth while the 1-meter model represents the shallow water depth. The 2-meter and 3-meter models showed increased fluid pressure in the region above the plate indicating that the rise in depth increased fluid pressure and stress on the front plate. Figure 36 compares the fluid pressure with different water depths. The stress, strain and displacement responded similarly like the fluid pressure for different water depths.

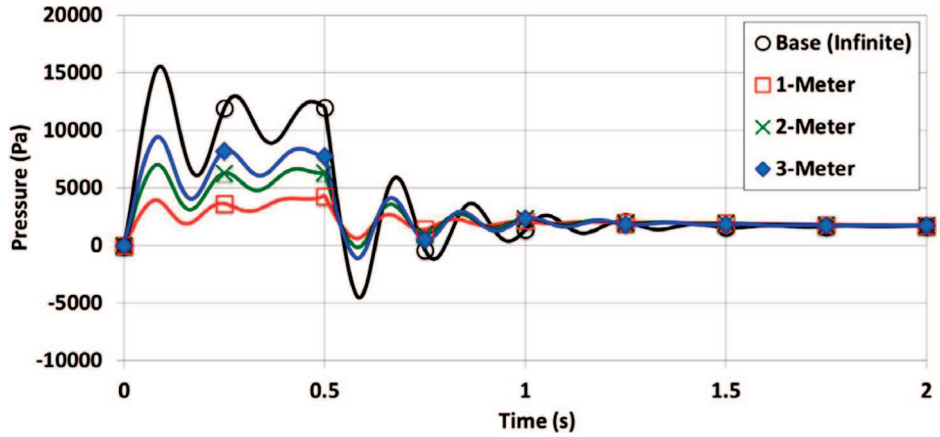

Figure 36: Comparison of average fluid pressure with different water depth from free surface

A maximum to steady state value comparison was also completed to facilitate a comparison of the base, 1-meter, 2-meter and 3-meter models. The base model received the highest ratio and was symmetric about the center. The 1-meter model the smallest ratio at the upper boundary point and increased along the plate toward its bottom boundary. The ratios for 2-meter and 3-meter models also tracked accordingly with depth. Additional models with different depths were also analyzed to draw a curve as shown in Fig. 37 which suggests that any water depth greater than 9 meters can be treated as the infinite depth in a practical sense when the water depth effect is considered on the ratio of the maximum to steady state values. The 1-meter model had the ratio of 2 approximately, and the ratio increased as a function of the water depth until it reached a plateau at around 9 meter. This result is similar with the data in Ref. [21] which investigated energy scavenging from tidal forces and reported that normalized velocity deficits in the water column decrease to near zero as depth exceeds 7 meters.

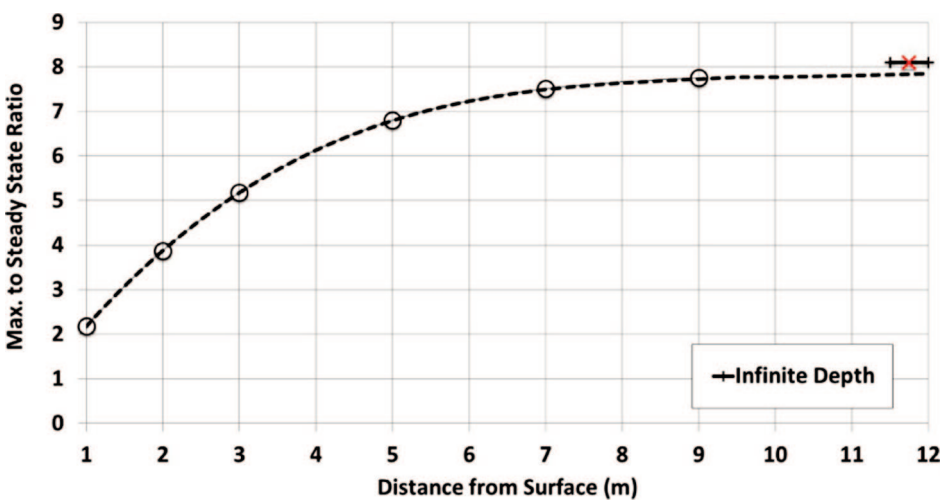

Figure 37: Plot of ratios of maximum to steady state stress/strain against water depth from free surface

6. SUMMARY AND CONCLUSIONS

A computational study was conducted to investigate dynamic responses and resultant stresses/strains occurring in composite structures which were submerged in water and subjected to transient fluid motions. After the computational model was validated against experimental data, a parametric study was undertaken to understand the effect of the transient fluid flow on composite structures. The parameters considered include variations in fluid accelerations during the transient phase; structural sizes, shapes, and material properties; and depth from the free surface of water.

The study showed that stresses were much greater during the transient acceleration phase than at the terminal steady state phase, as expected. The maximum stress during the transient phase is proportional to the acceleration magnitude, and any sudden change in acceleration also increased the maximum stress. As a result, the maximum stress occurred mostly at the first peak of the oscillatory response during the transient phase, which corresponded to the time when the structure had the first inward maximum deflection. However, when there were stops with zero speeds during the transient phase of motion, the maximum stress occurred at a later peak rather than the first peak.

The ratio of the maximum stress during the transient phase to the stress at the steady state phase was computed and compared. The results showed that the ratio was greater when the initial acceleration was larger and the terminal steady state velocity is lower. For example, when the acceleration was 8 m/s^2, the ratio was 16 while the acceleration was 2 m/s^2, the ratio was 4. The transient velocity profiles with more frequent stops also resulted in a larger ratio.

The structural sizes and shapes greatly influenced the stress ratio. A more hydrodynamic shape reduced the ratio. For example, the flat face cylinder had the ratio of almost 10 while the dome-shape face cylinder has the ratio of 4. On the other hand, the larger size of structure resulted in a higher stress ratio.

Even though the material properties of the structure did not affect the stress/strain ratio between the maximum and steady state values significantly, the maximum stress/strain magnitudes were influenced by the change in material properties. The lower density of the structure resulted in a higher maximum stress./strain under the same fluid flow. This suggests that lighter composite structures will endure larger stress when they travel underwater.

All the previous cases studied an infinitely large fluid domain without considering any boundary layer effect. The other study considered the free surface with zero pressure. Then, the effect of the depth of the location of the structure from the free surface was examined. The study showed that the free surface reduced the stress ratio. For example, the structure was placed 1 meter below the free surface, the stress ratio was approximately 2. As the water depth became more than 9 meters, the stress ratio was very close to that for the infinite depth.

Because increased hydraulic forces and resultant stresses are experienced during a transient fluid velocity, it is necessary to include this transient force in maritime design applications. Unmanned underwater vehicles can readily incorporate the use of composite materials. Such underwater vehicles generally travel at slow speeds below five knots (2.5 m/s) and could be exposed to similar acceleration transients as those modeled in this research, especially step acceleration and monotonic acceleration cases. The results of this study indicate the need to include transient forces in the design process as well as to determine the operating conditions of an underwater vehicle for the optimal transient velocity profiles.

ACKNOWLEDGEMENT

This work was supported by the ONR (Office of Naval Research) Solid Mechanics Program (Code 332). The program manager is Dr. Yapa Rajapakse. Special thanks go to Lt. Scott Millhouse, USN for conducting the experiment.

REFERENCES

[1] Loth, E. "Drag of non-spherical solid particles of regular and irregular shapes", *Power Technology*, Vol. 182, Issue 10, March 2008, pp. 342–353.

[2] Lund, K. O. "Low Reynolds-number moment on asymmetric bodies", *Experimental Thermal and Fluid Science*, Vol. 24, Issue 1–2, March 2001, pp. 61–66.

[3] Bagnold, R. A. "Experiments on a gravity-free dispersion of large solid spheres in a Newtonian fluid under shear", *Proc. Royal Society London A*, Vol. 225, No. 1160, August 1954, pp. 49–63.

[4] Kurose, R. and Komori, S. "Drag and lift forces on a rotating sphere in a linear shear flow", *J. Fluid Mech.*, Vol. 384, 1999, pp. 183–206.

[5] Lawrence, C. J. and Weinbaum, S. "The unsteady force on a body at low Reynolds number; the axisymmetric motion of a spheroid", *J. Fluid Mech.*, Vol. 189, 1988, pp. 463–489.

[6] Lawrence, C. J. and Mei, R. "Long-time behavior of the drag on a body in impulsive motion", *J. Fluid Mech.*, Vol. 283, 1995 pp. 307–327.

[7] Lovalenti, P. M. and Brady, J. F. "The temporal behavious of the hydrodynamic force on a body in response to an abrupt change in velocity at small but finite Reynolds number", *J. Fluid Mech.*, Vol. 293, 1995, pp. 35–46.

[8] De Bruyn, J. R. "Transient and steady-state drag in foam", *Rheol. Acta.*, Vol. 44, 2004, pp. 150–159.

[9] Sun, M., Saito, T., Takayama, K. and Tanno, H. "Unsteady drag on a sphere by shock wave loading", *Shock Waves*, 2005, Vol. 14, Issue 1–2, 2005, pp. 3–9.

[10] Tehrani, K., Rakheja, S. and Sedaghati, R. "Analysis of the overturning moment caused by transient liquid slosh inside a partially filled moving tank," Proceedings of the Institution of Mechanical Engineers, Part D: *Journal of Automobile Engineering*, March 2006, pp. 220–289.

[11] Liu, W. K. and Chang, H. C. "Efficient computational procedures for long-time duration fluid0structure interaction problems", *Journal of Pressure Vessel Technology*, Vol. 106, No. 4, November 1984, pp. 317–322.

[12] Pai, N. C., Bhattacharyya, S. K. and Sinha, P. K. "Non-linear coupled slosh dynamics of liquid-filled laminated composite containers: a two dimensional finite element approach", *Journal of Sound and Vibration*, Vol. 261, Issue 4, April 2003, pp. 729–749.

[13] Wiggert, D. C. and Tijsseling, A. S. "Fluid transients and fluid-structure interaction in flexible liquid-filled piping", *Appl. Mech. Rev.,* Vol. 54, No. 5, Sepember 2001, pp. 455–481.

[14] Tokuda, N., Sakurai, T. and Teraoku, T. "Sloshing analysis method using existing FEM structural analysis code", *Journal of Pressure Vessel Technology,* Vol. 117, No. 3, August 1995, pp. 268–272.

[15] Belytschko, T. and Karabin, M. and Lin, J. I. "Fluid-structure interaction in waterhammer response of flexible piping", *Journal of Pressure Vessel Technology,* Vol. 108, No. 3, August 1986, pp. 249–255.

[16] Kwon, Y. W., Priest, E. M. and Gordis, J. H. "Investigation of Vibrational Characteristics of Composite Beams with Fluid-Structure Interaction", *Composite Structures*, Vol. 105, November 2013, pp. 269–278.

[17] Kwon, Y. W., Violette, M. A., McCrillis, R. D. and Didoszak, J. M. "Transient Dynamic Response and Failure of Sandwich Composite Structures under Impact Loading with Fluid Structure Interaction", *Applied Composite Materials*. Vol. 19, No. 6, 2012, pp. 921–940.

[18] Craugh, L. E. and Kwon, Y. W. "Coupled Finite Element and Cellular Automata Methods for Analysis of Composite Structures with Fluid-Structure Interaction", *Composite Structures*, Vol. 102, August 2013, pp. 124–137.

[19] Kwon, Y. W. and Conner, R. P. "Low Velocity Impact on Polymer Composite Plate in Contact with Water", International Journal of Multiphysics, Vol. 6, No. 3, 2012, pp. 179–197.

[20] Lee, H. *Finite Element Simulations with ANSYS Workbench 14*, Mission, KS: SDC Publications, 2012.

[21] Sun, X. "Numerical and experimental investigation on tidal and current energy extraction," Ph.D. dissertation, University of Edinburgh, United Kingdom, 2008.